Oxygen-vacancies-engaged efficient carrier utilization for the photocatalytic coupling reaction

Xue Yang [a,b], Huilin Tao [c], Wan Ru Leow [d], Jingjun Li [a,b,c], Yanxi Tan [a,b], Yongfan Zhang [c], Teng Zhang [a,b], Xiaodong Chen [d], Shuiying Gao [a,b,*], Rong Cao [a,b,*]

[a] State Key Laboratory of Structural Chemistry, Fujian Institute of Research on the Structure of Matter, Chinese Academy of Sciences, Fuzhou 350002, China
[b] University of Chinese Academy of Science, Beijing 100049, China
[c] College of Chemistry, Fuzhou University, Fuzhou 350108, China
[d] Innovative Center for Flexible Devices, School of Materials Science and Engineering, Nanyang Technological University, 50 Nanyang Avenue, Singapore 639798, Singapore

ARTICLE INFO

ABSTRACT

Defects can greatly optimize the solar light harvesting capability and electronic structure of oxide materials. However, it remains challenging to achieve a defect engineering strategy under mild conditions. Meanwhile, the simultaneous exploitation of photogenerated holes (h^+) and electrons (e^-) to promote both photooxidation and photoreduction in a coupled system has rarely been reported. For the first time, we reveal an oxygen-vacancies-mediated photocatalytic strategy in which the electrons and holes are fully utilized for nitrobenzene reduction coupled with benzyl alcohol oxidation. The oxygen vacancies (OVs) generated *in situ* on the surface of TiO_2 greatly extend light absorption into the visible region and promote the photogenerated electron transport for efficient photocatalysis. The experimental and theoretical results together indicate that chemisorption on the TiO_2 surface decreases the oxidation potential of benzyl alcohol and causes an upward shift in its HOMO, which facilitates the oxidation reaction of benzyl alcohol to benzaldehyde. The *in situ* generated surface OVs also act as a bridge to enable the trapping and transferring of the photoinduced electrons to the nitrobenzene. This work provides a new perspective of utilizing the chemisorption between the reactant and catalyst to achieve a defect engineering strategy for synergetic photocatalysis.

© 2019 Published by Elsevier Inc.

1. Introduction

The application of photocatalysis in selective organic transformations is a promising strategy for synthetic chemistry, as such process tend to be cost-effective, photo-stable and nontoxic [1–5]. However, most traditional semiconductor materials absorb only ultraviolet light due to its wide band-gap, which greatly limits its application. Hence, developing an eco-friendly strategy for expanding the absorption range continues to attract great interest. Oxygen vacancies (OVs) possess great potential for extending the light response into visible region and manipulating the mechanism pathways of photocatalytic reactions [6–11]. A pioneering work reported the preparation of "black" TiO_2 with defective sites through hydrogenation under drastic conditions (20 bar H_2 flow at 500 °C for 5 days) [12]. However, it remains challenging to introduce OVs under mild conditions. Additionally, conventional strategies such

as H_2 reduction for OVs generation are always associated with bulk defects, which potentially act as electron-hole recombination centers and limit the photocatalytic activity [13]. If the OVs can be generated *in situ* during the photocatalytic process and serve as antennas to absorb visible light, the assembly would be simplified significantly. The most recent reports found that visible-light-sensitive surface complexes can be formed between semiconductors and specific colorless substrates, such as benzyl alcohols, benzylamines and their derivatives, thus providing another approach to tune the defects in classic wide-bandgap photocatalysts such as TiO_2, Nb_2O_5, and ZnO [14,15]. Xu et al. reported that OVs can be generated through surface complexation between benzyl alcohol and the TiO_2 surface, but lead to the deactivation of TiO_2 [16]. Evidently, the concept of using surface complexes as the active center to achieve a defect engineering strategy without damaging the photocatalyst stability is still in its infancy.

The transfer pathway and lifetime of photogenerated electron-hole pairs are vital to the efficiency and selectivity of photocatalysis [17–20]. Traditional methods to inhibit recombination of photogenerated electron-hole pairs involve removing the holes

with sacrificial reagents, such as triethanolamine, Na_2SO_3 or methanol [21–23]. Though both electrons and holes possess excellent reducing and oxidizing capacities, respectively, the simultaneous exploitation of photogenerated holes and electrons to promote both photocatalytic reactions of oxidation and reduction in a single system has rarely been reported. Jiang's group recently demonstrated a strategy in which hydrogen was produced by the photogenerated electrons while the benzylamine oxidation was catalyzed by the holes over a Pt/PCN-777 composite [24]. The recent development of such coupled systems that fully exploit photoexcited electrons and holes has recently attracted great interest for the greater utility of photocatalytic materials [25–27].

The selective oxidation of alcohols to benzaldehydes is a promising approach for the production of high-value-added chemicals and products [28–31]. Meanwhile nitrobenzene is an electron-accepting substrate that can be reduced by high-negative-value conduction band electrons [32–35], but it still remains challenging to improve its low conversion and selectivity. Here, experimental characterizations in conjunction with DFT calculations reveal that OVs *in situ* induced through surface complexation, which broaden the light absorption range and act as a bridge to enable the transfer of the photoinduced electrons. The benzyl alcohol oxidation half reaction mediated by photogenerated holes is desired. Simultaneously, rather than recombine with their counterpart holes, efficient electron transport may occur from the TiO_2 conduction band to nitrobenzene for the other half reaction. Moreover, the TiO_2 with OVs demonstrate high activity and long stability in this coupled system. This work provides a new perspective on utilizing the complexation between the reactants and catalyst to achieve a defect engineering strategy for synergic photocatalysis.

2. Experimental

2.1. Materials and methods

All of the reagents were purchased from commercial suppliers and used without further purification. Anatase TiO_2 microspheres were prepared by the microwave-assisted method [36]. Typically, 3.6 mL of $TiCl_4$ solution (14% in dichloromethane) was slowly added into a mixture of 24 mL of methanol and 12 mL of acetic acid under magnetic stirring in an ice bath. The clear mixture solution was then transferred into a 20 mL vial for microwave reaction. The synthesis was performed in a 400-W microwave oven heated at 130 °C for 1 h (Initiator 8 EXP, Biotage Corp). The white TiO_2 powders could be obtained after washing several times with ethanol and drying at 70 °C under vacuum. The fluorinated TiO_2 was prepared by adding 10 mM NaF into a 0.5 g/L TiO_2 aqueous solution, evaporating the water from the suspension and drying at 70 °C for 2 h.

Powder X-ray diffraction (XRD) was recorded by a Rigaku Mini-Flex 600 diffractometer with Cu Kα irradiation. The morphologies of the samples were examined by scanning electron microscopy (SEM, JSM6700) and high-resolution transmission electron microscopy (TEM, JEM2010). The Brunauer-Emmett-Teller (BET) specific surface area of the samples was analyzed by nitrogen adsorption in a Micromeritics ASAP 2020 apparatus. UV–visible diffuse reflectance spectroscopy was measured by a Shimadzu UV-2600 with $BaSO_4$ as the reference and transformed to the absorption spectra according to the Kubelka-Munk relationship. The EPR spectra were obtained on a Bruker-BioSpin E500 spectrometer at room temperature. The irradiation source was same light source used in our photocatalytic experiments described below. A pump wavelength of 400 nm was used for the time-resolved photoluminescence (TRPL), which originates from the frequency-doubled 800 nm laser pulses generated from a Coherent Libra Regenerative Amplifier using a Beta Barium Borate (BBO) crystal.

2.2. Typical experimental procedure for photocatalytic test

In a typical procedure, 40 mg of TiO_2, 31 μL (0.3 mmol) of benzyl alcohol and 10 μL (0.1 mmol) of nitrobenzene were added into 10 mL of reagent grade benzotrifluoride (BTF), n-dodecane was used as an internal standard. The mixture was evacuated and back-filled with N_2 (1.0 atm) five times to completely remove air and allowed to stir for 30 min in the dark. The reaction mixture was then magnetically stirred at 800 rpm and illuminated by the 300-W Xenon Illuminator System with an CM 1 filter in the wavelength region of 380–760 nm. At a certain time after the photocatalytic reaction, an aliquot of the reaction solutions (60 μL) were pulled out, filtered by a one-time plastic filter and diluted by 0.5 mL ethanol for gas chromatograph analysis (Agilent 7890A equipped with an FID detector). The conversion of alcohol, nitrobenzene, and yield of aldehyde and aniline were defined as follows:

$$\text{Conversion}\,(\%) = [(C_0 - C_r)/C_0] \times 100 \tag{1}$$

$$\text{Yield}\,(\%) = C_t/C_0 \times 100 \tag{2}$$

C_0 is the initial concentration of reactant; C_r and C_t are the remaining concentrations of reactant and target product in the reaction system. In particular, the yield of the Schiff base is based on the initial concentration of nitrobenzene. The products were confirmed by gas chromatography mass spectrometry (430 GC Varian, USA) and comparing their retention times with those of standard samples. When the photocatalytic experiments completed, the reaction mixtures were centrifuged to separate the photocatalyst from reaction mixture and dried in an oven at 70 °C overnight for the following cycling photoactivity test and further characterization. For clarity, the catalysts after the photocatalytic reaction in the coupled systems were denoted as used TiO_2, unless otherwise stated. To explore the scope of our catalyst, the benzyl alcohol was replaced by 0.3 mmol of different diverse aromatic alcohols while other experimental parameters were remained. Controlled photoactivity experiments using radical scavengers, triethanolamine (0.3 mmol) as the scavenger for photogenerated holes, and CCl_4 (0.3 mmol) as the scavenger for electrons, were performed in a similar manner to the above photocatalytic experiment with the radical scavengers added to the reaction system.

2.3. Electrochemistry measurements

The catalyst-modified electrode was prepared on a fluorine-doped tin oxide (FTO) glass. The FTO slide was previously protected using Scotch tape to ensure the exposed area of the working electrode was controlled at 1.0 cm². The FTO slide was dip coated with 40 μL of slurry, which was obtained from the mixture of 10 mg of photocatalyst, 0.7 mL of DMF and 0.3 mL of alcohol under sonication for a certain time. After air drying, the working electrode was further dried at 150 °C for 2 h to improve adhesion. All the electrochemistry measurements were carried out using a ZM6ex electrochemical station (Zahner, Germany) in a three-electrode quartz cell. The Mott-Schottky and photocurrent analyses were measured in a 0.2 M Na_2SO_4 aqueous solution and purged with N_2 before the measurement. The light irradiation source was the same as that used in the aforementioned photoactivity tests. Cyclic voltammetry was carried out using 0.2 M solution of tetra-n-butylammonium hexafluorophosphate (TBAPF6) in CH_3CN as the supporting electrolyte. A glassy carbon electrode was used as the working electrode for the measurement of the oxidative potential of benzyl alcohol.

2.4. Computational methods

All the calculations were performed by the first-principles calculations based on the density functional theory (DFT) [37,38]. Computational simulations of the TiO$_2$ (1 0 1) surface and the benzyl alcohol adsorption were conducted with the Vienna ab initio simulation package (VASP). The projector augmented wave (PAW) method [39] was used to describe the electron-ion interaction. The generalized gradient approximation in the Perdew-Burke-Ernzerhof [40,41] formalism (GGA-PBE) was used to account for the exchange and correlation interactions between electrons. An energy cut-off of 450 eV was used, and a 3 × 3 × 1 k-point mash was used to sample the Brillouin zone [42] for the gas phase molecules and TiO$_2$ (1 0 1) surface. The TiO$_2$ surface has dimensions of 10.89 × 11.33 × 25 Å, with three slab layers and a total of 108 atoms. The valence band maximum (VBM) of TiO$_2$ was confirmed by the value of the work function, and the conduction band minimum (CBM) was defined as VBM with the addition of a band gap. The Gaussian09 package was used for the calculations of the benzyl alcohol and the nitrobenzene molecules. The B3LYP functional with a 6-31*G basis set was used for the calculations. The vacuum level was used to locate the absolute energy level.

3. Results and discussion

The TiO$_2$ used in this work was synthesized using a facile one-step microwave-assisted method. The electron microscope images revealed the microsphere morphology of TiO$_2$ (Fig. 1a–b). The XRD patterns indicated that the TiO$_2$ samples were indexed to anatase phase (Fig. 1c), which is a better photocatalyst than rutile TiO$_2$ [43]. The N$_2$ sorption experiment on the prepared TiO$_2$ indicated a Brunauer-Emmett-Teller (BET) surface area as high as

213.17 m^2/g and meso-pores with a diameter of 3.60 nm (Fig. 1d). It is worth mentioning that large pore sizes are favorable for the exposure of active sites and efficient transfer of photogenerated carriers.

The photooxidation of benzyl alcohol to benzaldehyde and the photoreduction of nitrobenzene to aniline were realized simultaneously under mild reaction conditions (Table 1). The benzyl alcohol and nitrobenzene reached a desirable conversion of 100% under standard conditions (entry1, Table 1), where TiO$_2$ and light irradiation are both essential (entries 2–3, Table 1). More interestingly, the photocatalytic products of benzaldehyde and aniline once generated can be further convert into Schiff bases, which have wide application in medical science and the chemical industry. Various different reaction conditions were then explored for comparison. When altering the reaction atmosphere to ambient air (entry 4, Table 1), the conversion of benzyl alcohol reached 100% but no conversion of nitrobenzene was obtained. This was because the photoexcited electrons are transferred to O$_2$ in air (an electron acceptor) rather than to nitrobenzene, thus preventing the reduction of the latter. No color change was observed when P25 was used as the photocatalyst, indicting no complexation was formed between P25 and benzyl alcohol. As a result, P25 showed negligible photocatalytic ability in such a coupled reaction (entry 5, Table 1). In our report, the mesoporous TiO$_2$ prepared by a one-step microwave-assisted esterification method exhibits good photocatalytic ability. This is related to surface properties of TiO$_2$. As seen from Infrared spectrum (Fig. S10), the band at 3274 cm^{-1} can be ascribed to the stretching vibrations of —OH, while the bands at 1618 cm^{-1} and 1524 cm^{-1} correspond to the symmetric and asymmetric vibrations of COO$^-$ [36]. The presence of —OH and COO$^-$ peak is very helpful to benzyl alcohol adsorbed on the TiO$_2$ by the surface complexation. The addition of a hole scavenger such
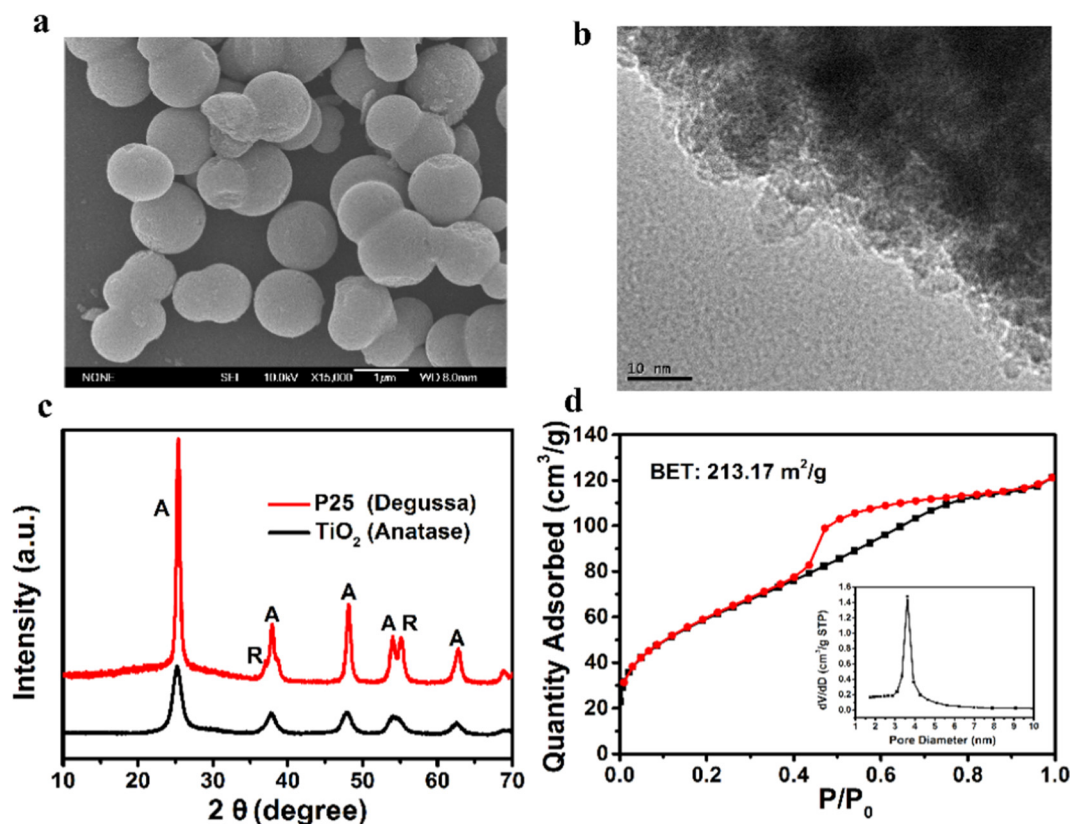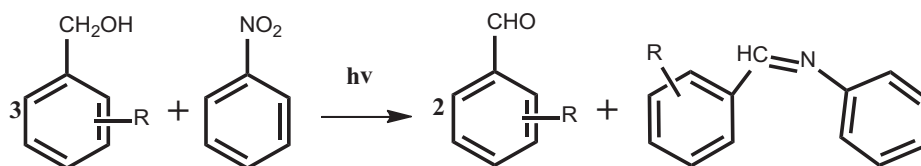

Fig. 1. SEM image (a) and TEM (b) image of the synthesized TiO$_2$. (c) XRD patterns of anatase TiO$_2$ and Degussa P25 (A = anatase, R = rutile). (d) Nitrogen sorption isotherms at 77 K for TiO$_2$. The insert is the DFT pore size distribution for TiO$_2$.

Table 1
Control experiments for the coupled system of benzyl alcohol oxidation and nitrobenzene reduction under irradiation for 3 h.

Entry	Catalyst	Oxidation Conversion (%)	Reduction Conversion (%)	Schiff base Yield[a] (%)
1[b]	TiO_2	100	100	100
2[c]	TiO_2	trace	trace	trace
3	Blank	0	0	0
4[d]	TiO_2	100	0	0
5	P25	trace	trace	Trace
6[e]	TiO_2	80	100	100
7[f]	TiO_2	100	38	38
8[g]	TiO_2	56	51	51

[a] Yield of the Schiff base is based on the initial concentration of nitrobenzene.
[b] Standard conditions: 40 mg of TiO_2, 0.3 mmol of benzyl alcohol, 0.1 mmol of nitrobenzene, 10 mL of benzotrifluoride, 300 W Xe lamp, 1 atm of N_2 for 3 h.
[c] Without irradiation.
[d] Air atmosphere instead of nitrogen atmosphere.
[e] triethanolamine (0.3 mmol) was added into the coupled reaction system as a hole scavenger.
[f] CCl_4 (0.3 mmol) was added as a photoelectron scavenger.
[g] Xe lamp coupled with a light filter ($\lambda > 420$ nm).

as triethanolamine into the coupled reaction system diminished the oxidation of benzyl alcohol, but the conversion of nitrobenzene was maintained, indicating that the photoexcited holes were the primary active species for the half oxidation reaction (entry 6, Table 1). Additionally, upon the addition of CCl_4 that scavenges photoelectrons into the coupled system (entry 7, Table 1), the conversion of nitrobenzene was reduced from 100% to 38%. This suggests the importance of photogenerated electrons in enabling the reaction. The photocatalytic selective oxidation of benzyl alcohol to benzaldehyde is a 2-electron and 2 H^+ released oxidation reaction. While the nitrobenzene was reduced to aniline by consuming six electrons and six H^+. As a result, the amount of benzyl alcohol in this reaction system must be 3 times the amount of nitrobenzene. From here, we can see that coupling two such challenging reactions into one system is an effective way to fully utilize photoexcited electron-hole pairs. Under the irradiation of above 420 nm, our prepared TiO_2 also exhibits a desired photocatalytic activity for the selective photocatalytic synthesis of Schiff bases (entry 8, Table 1, Fig. S14). Besides, the decrease of the photocatalytic activity can be ascribed to the decreased photon energy above 420 nm as compared to the light region above 380 nm.

It is interesting to note that the UV–vis spectrum of TiO_2 after photocatalytic reaction showed absorption in the visible region (denoted as used TiO_2), which was accompanied by a distinct colour change from white to yellow (Fig. 2b). According to the literature, this phenomenon is assigned to the ligand-to-metal (LMCT) charge transfer in the complex formation between benzyl alcohol and —OH on the TiO_2 surface [44]. When TiO_2 was treated with an aqueous solution of NaF [39], the intensity of the characteristic —OH (3281 cm^{-1}) peak was diminished upon fluorinating the surface of TiO_2 (Fig. S13). As a result, the surface complex formation between TiO_2 and benzyl alcohol was eliminated and the photocatalytic activity of the resulting F-TiO_2 was significantly inhibited (Fig. S1). The colour change of the TiO_2 powders after the photocatalytic reaction not only was consistent with the efficient visible light absorption but also suggested the existence of surface defects on TiO_2. The electron paramagnetic resonance (EPR) spectroscopy has been conducted to verify this suggestion. The substrate of benzyl alcohol (10 mM) was added to fresh aqueous TiO_2 suspension (1 g/L). The benzyl alcohol-adsorbed TiO_2 powder was obtained

by filtering the suspension and drying in an oven at 80 °C. As shown in Fig. S11, (ESI†) no color change was observed when the fresh photocatalyst adsorbs the benzyl alcohol. Similarly, Schiff base was added to fresh aqueous TiO_2 suspension (1 g/L) in order to demonstrate the Schiff base effect on the EPR signal of the sample. It was found that benzyl alcohol and Schiff base absorbed on fresh TiO_2 powders showed no distinct EPR signals (Fig. S12). It's also worth pointing out that the light irradiation is a necessary factor in determining the color change of photocatalyst from white to yellow. This indicates that the EPR signal of the sample is from benzyl alcohol absorbed on TiO_2 surface under the light irradiation. There was no EPR signal for the fresh TiO_2 (Fig. 2c) and P25 (Fig. S2) both in the dark and under visible light irradiation, because such samples were only photoresponsive in the UV region. In contrast, the samples of used TiO_2 from the coupled system (Fig. 2c) and from the individual reaction of benzyl alcohol oxidation (Fig. S3) showed distinct EPR signals at g = 2.004, owing to the electrons trapped in the oxygen vacancies (OVs) [45]. Furthermore, illumination, compared to dark conditions, significantly enhanced the OVs signals, indicating efficient photoinduced generation of the charge carrier pairs. The time-resolved photoluminescence (TRPL) spectra in Fig. 2d strikingly showed that the emission induced by the OVs exhibits a much longer lifetime ($\sim$1.96 ns) than the emission of the fresh TiO_2 sample ($\sim$0.98 ns), suggesting that the OVs on the TiO_2 surface accelerate the trapping and transferring of the photoinduced electrons, which should be beneficial for the subsequent photocatalysis.

To help validate the experimental results and provide fundamental insights into the effect of benzyl alcohol adsorbed on the TiO_2 surface, the first-principles calculations based on the density functional theory (DFT) were performed (Fig. 3). An anatase TiO_2 (1 0 1) surface was simulated, which contains 2-fold coordinated oxygen anions (O_{2c}) and O_{3c} atoms, as well as 5-fold coordinated Ti cations (Ti_{5c}) and fully coordinated Ti_{6c} atoms. The O_{2c} atom will coordinate with the Ti_{5c} and Ti_{6c} atoms with bond length of 1.84 Å and 1.87 Å, respectively (Fig. 3a). Once the benzyl alcohol adsorbed on the TiO_2 surface, the interaction between the Ti_{6c} and O_{2c} atoms will be weakened due to the hydrogen-bonding interaction between the hydroxyl group of benzyl alcohol and the bridging oxygen atom. As a result, the Ti-O bond length will be weakened
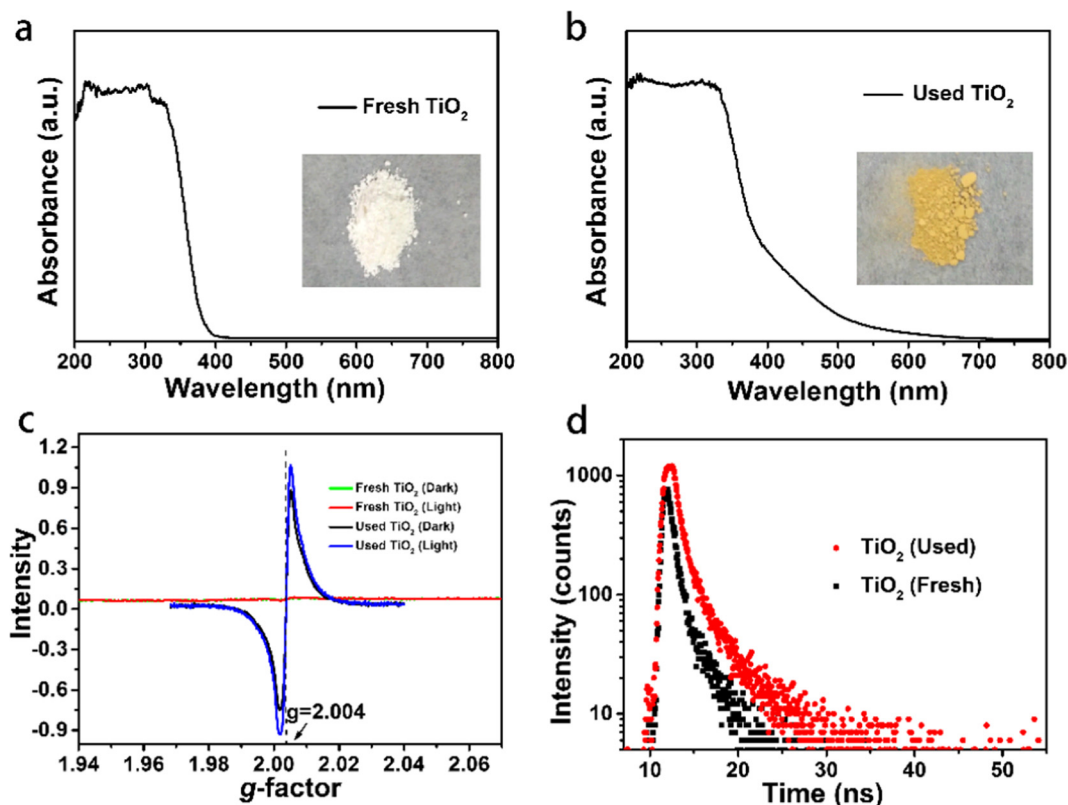
Fig. 2. (a) UV–vis spectra of fresh TiO₂, and used TiO₂ (b). (c) EPR signals of the fresh TiO₂, and used TiO₂ after photocatalytic reaction in the coupled system in the dark or under light irradiation. (d) Decay kinetics of TRPL (time-resolved photoluminescence) signals of the TiO₂ before and after photocatalytic reaction.
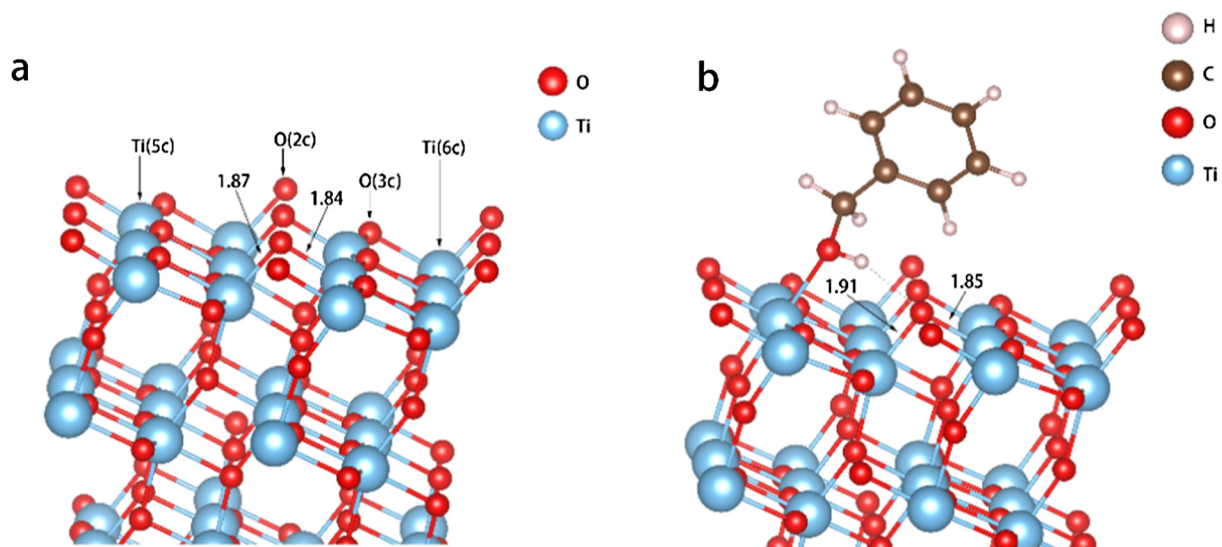

Fig. 3. (a) The optimized structure of the anatase TiO₂ (1 0 1) surface. (b) The benzyl alcohol adsorbed on the TiO₂ (1 0 1) surface.

and elongated by ~0.04 Å (Fig. 3b). This calculation result agrees well with the EPR spectroscopic results and elucidates the formation mechanism of surface OVs on the anatase TiO₂ (1 0 1).

Electrochemical Mott-Schottky plots were employed to glean more direct evidence on OVs. In Fig. 4a, the positive slopes of the C^{-2}-V curves at frequencies of 500, 800, and 1500 Hz demonstrated that the TiO₂ is a characteristic n-type semiconductor. The flat band values determined from the intersection of fresh TiO₂ were approximately ca. −0.52 V (vs. Ag/AgCl). However, a more negative

flat band of −0.97 V (vs. Ag/AgCl) was measured for the used TiO₂ (Fig. 4b). It has been generally believed that for n-type semiconductors, the flat-band potential (quasi-Fermi level) is located just 0.1 V lower than the conduction band minimum. More specifically, the conduction band minimum of TiO₂ before and after reaction were −0.42 V and −0.87 V (vs. Ag/AgCl) [46], respectively. It has been generally recognized that the localized electronic states of OVs typically lying below the conduction band that lower the Schottky barrier of semiconductors and facilitate interfacial
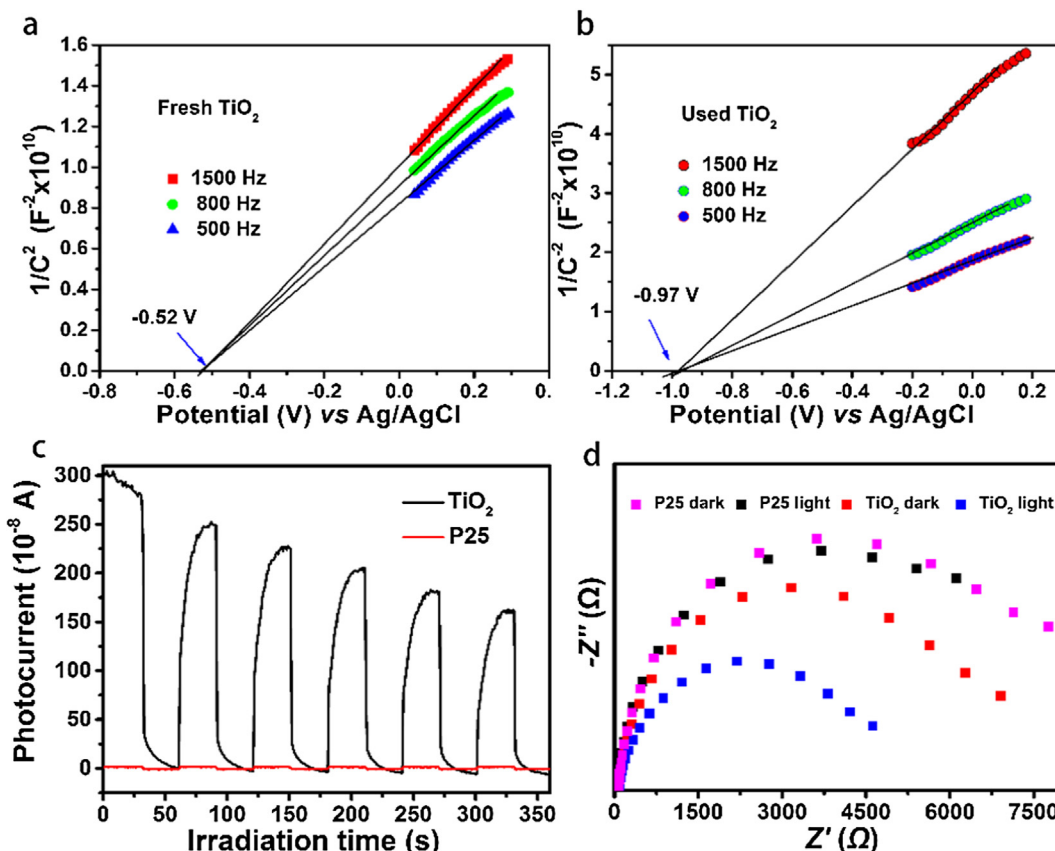
Fig. 4. Mott-Schottky plots for TiO₂ (a) and used TiO₂ (b) in 0.2 M Na₂SO₄ aqueous solution. (c) Photocurrent tests and (d) EIS plots of the prepared TiO₂ and commercial P25.

electrons transfer. This phenomenon not only jointly confirms the existence of OVs, but also indicates the thermodynamic feasibility of nitrobenzene reduction (-0.69 V vs. Ag/AgCl). Furthermore, the rapid charge separation efficiency was also proved by photocurrent and electrochemical impedance spectroscopy (EIS) measurements. A higher photocurrent response of TiO₂ indicted the more rapid transfer of photoinduced e⁻-h⁺ pairs (Fig. 4c), thus significantly improving the photocatalytic efficiency. In addition, the response of anatase TiO₂ indicated a smaller radius and a lower resistance in charge transportation than those of commercial P25 (Fig. 4d), signifying more efficient separation efficiency of photogenerated carriers. These results also matched well with the aforementioned catalytic activity order.

It is significative to explore the reaction mechanism behind two half reactions. We have further calculated the potential diagram of the substances involved with respect to normal hydrogen electrode (NHE) potential. The vacuum level was calculated by DFT, which is corrected by the values of the vacuum level of hydrogen and the electrode potential reduced by hydrogen. The reduction potential with E_{NHE} (H⁺/H₂) = -4.5 V was appointed as zero point [47]. As presented in Fig. 5a–c, the conduction band minimum (CBM) of TiO₂ became more negative (-1.25 V) after benzyl alcohol adsorption. It is obvious that nitrobenzene (NB) act as an electron acceptor and generate reducing reaction. Meanwhile, the Highest Occupied Molecular Orbital (HOMO) of benzyl alcohol (BnOH) transform into localized occupied state after adsorbing on the TiO₂ (1 1 0) surface. In this way, it is theoretically feasible for photooxidation of benzyl alcohol.

Furthermore, the oxidation potential of benzyl alcohol will be decreased through surface complexation on the TiO₂ surface. As shown in Fig. 5d, the voltammogram of benzyl alcohol measured with a bare glassy carbon electrode showed an irreversible

oxidation peak at approximately +2.2 V vs Ag/AgCl. However, the use of a TiO₂-modified electrode brings about an additional oxidation feature at +1.0 V vs Ag/AgCl. This oxidation feature in accordance with calculation result and is suggestive of a chemisorbed surface interaction between benzyl alcohol and TiO₂. From both theoretical and experimental perspectives, the benzyl alcohol half oxidation reaction with the help of holes is desired.

An oxygen-vacancies-engaged mechanism (Fig. 6) was proposed using the knowledge from these experimental and theoretical studies. As mentioned above, the complexation the between benzyl alcohol and TiO₂ surface is supposed to extend the light absorption into visible region and produce the required electron-hole pairs. The oxidation potential of benzyl alcohol will decrease through chemisorption on the TiO₂ surface. The photoinduced benzyl alcoholic radicals may spontaneously release an electron together with a successive deprotonation to generate benzaldehyde. The surface OVs would act as a bridge to enable the trapping and transferring of the photoinduced electrons to the nitrobenzene. Eventually, the nitrobenzene was reduced to aniline by consuming six electrons and six protons. In other word, fully making use of the photogenerated charge carriers in one system rapidly promoted the separation and transfer efficiency of the photogenerated charge carriers, thus significantly improved the photocatalytic activity.

The stability of a photocatalyst is very meaningful for its practical application. Gratifyingly, the photocatalytic activity of TiO₂ is well maintained even after 5 cycles (Fig. 7a), indicting the excellent recyclability and photostability of TiO₂ in this coupled system. One concern has always been worried that the accumulation of surface adsorbed species, such as OVs and intermediates, will lead to the deactivation of photocatalysts. Here, the EPR experiment revealed that the intensity of the OVs signals showed a negligible
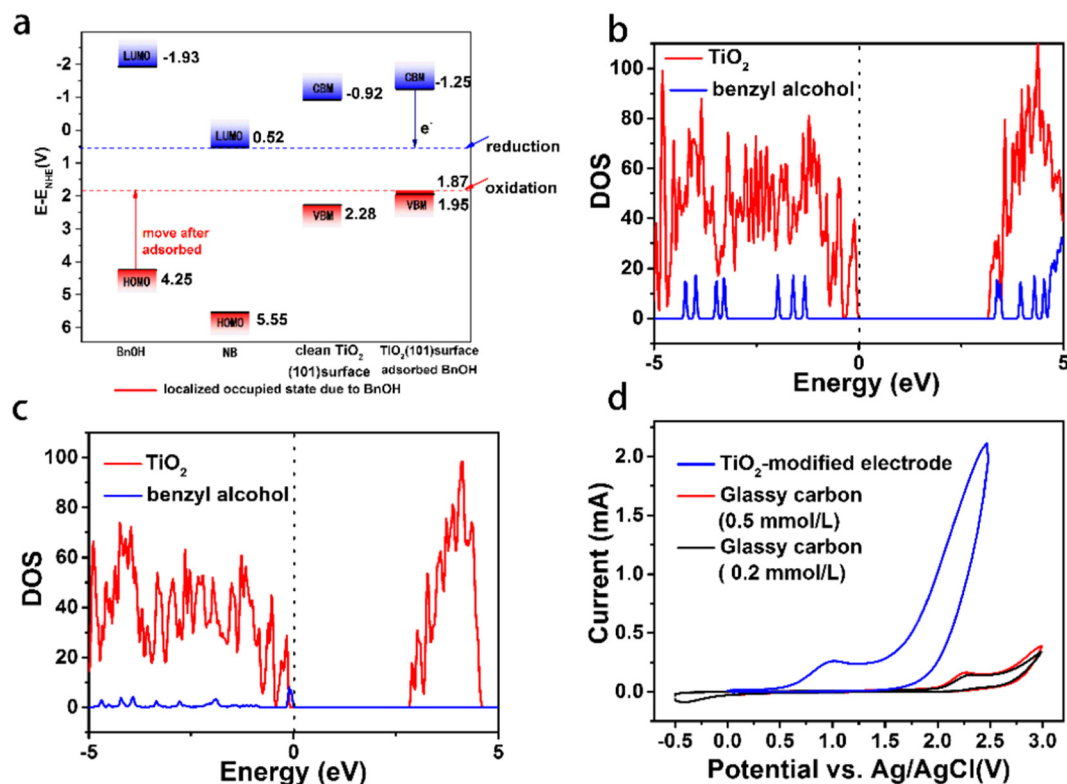
Fig. 5. (a) The potential diagram of benzyl alcohol (BnOH), nitrobenzene (NB), free TiO$_2$ and the chemisorbed surface complex with respect to normal hydrogen electrode (NHE) potential. (b) Total density of states (DOS) of benzyl alcohol and the bare TiO$_2$ surface. (c) Partial density of states (PDOS) of adsorbed benzyl alcohol and the TiO$_2$ surface when benzyl alcohol is chemisorbed. The dashed line indicates the formation of localized occupied states just above the VBM of TiO$_2$. (d) Cyclic voltammogram of benzyl alcohol with TiO$_2$-modified (blue) and bare electrodes with a concentration of 0.2 mM (black) and 0.5 mM (red).
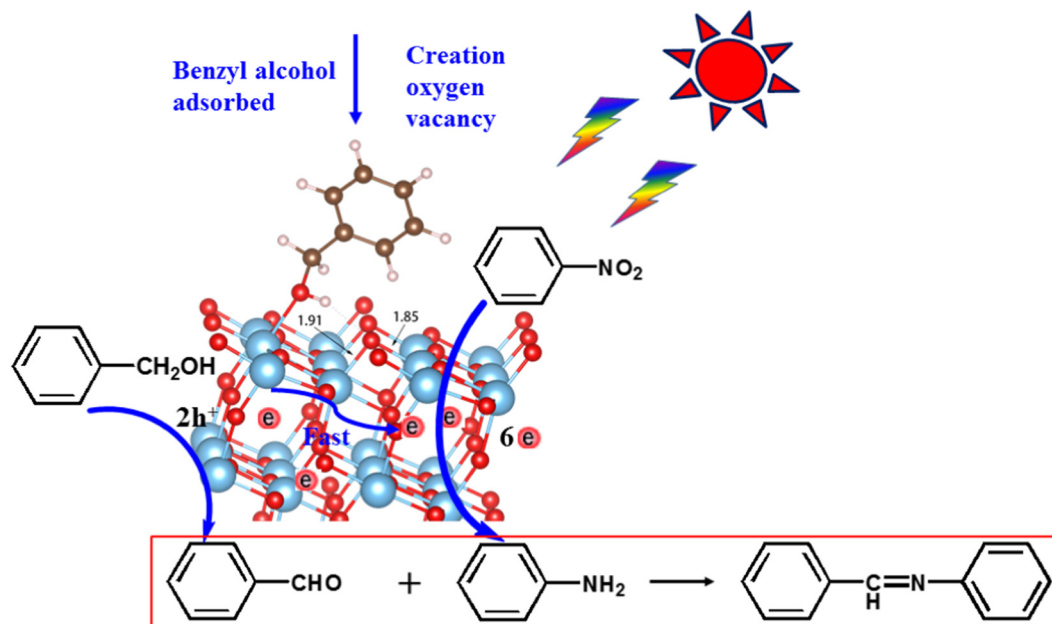
Fig. 6. Schematic illustration of the oxygen-vacancy-mediated photocatalytic mechanism of benzyl alcohol and nitrobenzene under visible light catalyzed by TiO$_2$.

change even after a longer irradiation time (Fig. 7b). Furthermore, the XRD patterns (Fig. S5) and morphology (Fig. S6) of anatase TiO$_2$ remained well before and after the reaction, indicating that only the surface of TiO$_2$ was involved in the photocatalytic reaction and suggesting the excellent recyclability of TiO$_2$.

Encouraged by the excellent catalytic performance of TiO$_2$ in the synergistic system of benzyl alcohol and nitrobenzene. Various aromatic alcohols were selected to further investigate the scope of this coupled reaction (insert N$_2$ atmosphere). As listed in Table 2, the conversion of aromatic alcohols para-substituted with
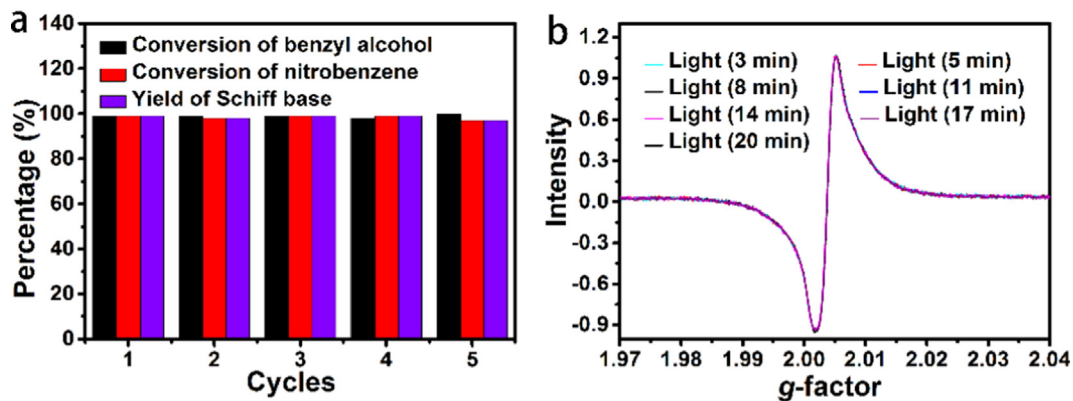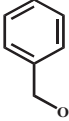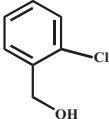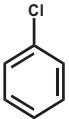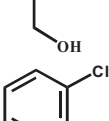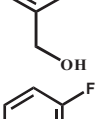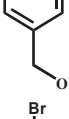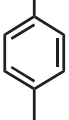
Fig. 7. (a) Recycling testing of TiO$_2$ towards photocatalytic benzyl alcohol oxidation coupled with nitrobenzene reduction under irradiation for 3 h. (b) EPR signals intensity of used TiO$_2$ under light irradiation for different time.

Table 2
Photocatalytic performance of various aromatic alcohols and nitrobenzene in the coupled system over TiO$_2$ for 3 h.[a]

Entry	Substrates	Oxidation Conversion (%)	Reduction Conversion (%)	Schiff base Yield[b] (%)
1		100	100	100
2		91.72	96.98	96.98
3		100	86.19	86.19
4		100	87.87	87.87
5		100	72.67	72.67
6		100	100	100
7		60.09	39.90	39.90

[a] Reaction conditions: 40 mg TiO$_2$, 0.3 mmol of aromatic alcohols, 0.1 mmol of nitrobenzene, 10 mL of benzotrifluoride, 300 W Xe lamp, 0.1 M Pa of N$_2$ for 3 h. n-dodecane was used as the internal standard.

[b] Yield of the Schiff base is based on the initial concentration of nitrobenzene.

electron-donating groups (—CH$_3$) (entry 7) was lower than those of the electron-withdrawing groups (—Cl, —F, —Br) (entries 2–6). In addition to the electronic effect, steric hindrance also leads to a lower activity of the reaction. 2-chlorine benzyl alcohol (entry 2) showed a lower conversion relative to 4-chlorine benzyl alcohol (entry 3), as the chlorine group in the ortho position provides greater steric hindrance around the O—H group. This phenomenon also indicated that surface complexation occurs between TiO$_2$ and a large variety of alcohols with different moieties.

4. Conclusion

In conclusion, a coupled photocatalytic system of aromatic alcohols oxidation and nitrobenzene reduction catalyzed by TiO$_2$ was demonstrated for the first time. The oxygen vacancies generated *in situ* on the surface of TiO$_2$, which would greatly extend the light absorption range and facilitate interfacial electron transfer for efficient photocatalysis. The coupled system simultaneously utilizes photogenerated e$^-$-h$^+$ pairs, thus rapidly boosting their separation and exhibiting satisfactory catalytic activity. Moreover, this strategy can well tolerate the substitution of alcohols substrates and exhibit excellent recyclability. This discovery will be a very promising concept guiding the pursuit of selective organic transformations in a coupled photocatalytic system utilizing surface chemisorption between the reactants and catalyst.

Notes

The authors declare no competing financial interest.

Acknowledgement

Appendix A. Supplementary material

Supplementary data to this article can be found online at https://doi.org/10.1016/j.jcat.2019.03.022.

References

[1] S. Linic, P. Christopher, D.B. Ingram, Plasmonic-metal nanostructures for efficient conversion of solar to chemical energy, Nat. Mater. 10 (2011) 911–921.

[2] J. Chen, J. Cen, X. Xu, X. Li, The application of heterogeneous visible light photocatalysts in organic synthesis, Catal. Sci. Technol. 6 (2016) 349–362.

[3] X. Lang, X. Chen, J. Zhao, Heterogeneous visible light photocatalysis for selective organic transformations, Chem. Soc. Rev. 43 (2014) 473–486.

[4] S. Zavahir, Q. Xiao, S. Sarina, J. Zhao, S. Bottle, M. Wellard, J. Jia, L. Jing, Y. Huang, J.P. Blinco, H. Wu, H.-Y. Zhu, Selective oxidation of aliphatic alcohols using molecular oxygen at ambient temperature: mixed-valence vanadium oxide photocatalysts, ACS Catal. 6 (2016) 3580–3588.

[5] S. Furukawa, T. Shishido, K. Teramura, T. Tanaka, Photocatalytic Oxidation of Alcohols over TiO$_2$ Covered with Nb$_2$O$_5$, ACS Catal. 2 (2011) 175–179.

[6] C. Mao, H. Cheng, H. Tian, H. Li, W.-J. Xiao, H. Xu, J. Zhao, L. Zhang, Visible light driven selective oxidation of amines to imines with BiOCl: does oxygen vacancy concentration matter?, Appl Catal. B: Environ. 228 (2018) 87–96.

[7] F. Lei, Y. Sun, K. Liu, S. Gao, L. Liang, B. Pan, Y. Xie, Oxygen vacancies confined in ultrathin indium oxide porous sheets for promoted visible-light water splitting, J. Am. Chem. Soc. 136 (2014) 6826–6829.

[8] J. Nowotny, M.A. Alim, T. Bak, M.A. Idris, M. Ionescu, K. Prince, M.Z. Sahdan, K. Sopian, M.A. Mat Teridi, W. Sigmund, Defect chemistry and defect engineering of TiO$_2$-based semiconductors for solar energy conversion, Chem. Soc. Rev. 44 (2015) 8424–8442.

[9] K.K. Banger, Y. Yamashita, K. Mori, R.L. Peterson, T. Leedham, J. Rickard, H. Sirringhaus, Low-temperature, high-performance solution-processed metal oxide thin-film transistors formed by a 'sol-gel on chip' process, Nat. Mater. 10 (2011) 45–50.

[10] H. Hirakawa, M. Hashimoto, Y. Shiraishi, T. Hirai, Photocatalytic conversion of nitrogen to ammonia with water on surface oxygen vacancies of titanium dioxide, J. Am. Chem. Soc. 139 (2017) 10929–10936.

[11] R. Kuriki, T. Ichibha, K. Hongo, D. Lu, R. Maezono, H. Kageyama, O. Ishitani, K. Oka, A. Stable, Narrow-gap oxyfluoride photocatalyst for visible-light hydrogen evolution and carbon dioxide reduction, J. Am. Chem. Soc. 140 (2018) 6648–6655.

[12] X. Chen, L. Liu, P.Y. Yu, S.S. Mao, Increasing solar absorption for photocatalysis with black hydrogenated titanium dioxide nanocrystals, Science 331 (2011) 746–750.

[13] M. Kong, Y. Li, X. Chen, T. Tian, P. Fang, F. Zheng, X. Zhao, Tuning the relative concentration ratio of bulk defects to surface defects in TiO$_2$ nanocrystals leads to high photocatalytic efficiency, J. Am. Chem. Soc. 133 (2011) 16414–16417.

[14] W.R. Leow, W.K. Ng, T. Peng, X. Liu, B. Li, W. Shi, Y. Lum, X. Wang, X. Lang, S. Li, N. Mathews, J.W. Ager, T.C. Sum, H. Hirao, X. Chen, Al$_2$O$_3$ surface complexation for photocatalytic organic transformations, J. Am. Chem. Soc. 139 (2017) 269–276.

[15] S. Higashimoto, N. Kitao, N. Yoshida, T. Sakura, M. Azuma, H. Ohue, Y. Sakata, Selective photocatalytic oxidation of benzyl alcohol and its derivatives into corresponding aldehydes by molecular oxygen on titanium dioxide under visible light irradiation, J. Catal. 266 (2009) 279–285.

[16] X. Pan, N. Zhang, X. Fu, Y.-J. Xu, Selective oxidation of benzyl alcohol over TiO$_2$ nanosheets with exposed 001 facets: catalyst deactivation and regeneration, Appl. Cataly. A: Gen. 453 (2013) 181–187.

[17] X. Lang, J. Zhao, X. Chen, Visible-light-induced photoredox catalysis of dye-sensitized titanium dioxide: selective aerobic oxidation of organic sulfides, Angew. Chem. Int. Ed. 55 (2016) 4697–4700.

[18] L. Chen, R. Luque, Y. Li, Controllable design of tunable nanostructures inside metal-organic frameworks, Chem. Soc. Rev. 46 (2017) 4614–4630.

[19] B. Ma, P.Y. Guan, Q.Y. Li, M. Zhang, S.Q. Zang, MOF-derived flower-like MoS$_2$@TiO$_2$ nanohybrids with enhanced activity for hydrogen evolution, ACS Appl. Mater. Inter. 8 (2016) 26794–26800.

[20] D. Tsukamoto, Y. Shiraishi, Y. Sugano, S. Ichikawa, S. Tanaka, T. Hirai, Gold nanoparticles located at the interface of anatase/rutile TiO$_2$ particles as active plasmonic photocatalysts for aerobic oxidation, J. Am. Chem. Soc. 134 (2012) 6309–6315.

[21] Y. Fu, D. Sun, Y. Chen, R. Huang, Z. Ding, X. Fu, Z. Li, An amine-functionalized titanium metal-organic framework photocatalyst with visible-light-induced activity for CO$_2$ reduction, Angew. Chem. Int. Ed. 51 (2012) 3364–3367.

[22] L. Lin, W. Ren, C. Wang, A.M. Asiri, J. Zhang, X. Wang, Crystalline carbon nitride semiconductors prepared at different temperatures for photocatalytic hydrogen production, Appl. Catal. B: Environ. 231 (2018) 234–241.

[23] J. Cai, Y. Zhu, D. Liu, M. Meng, Z. Hu, Z. Jiang, Synergistic effect of titanate-anatase heterostructure and hydrogenation-induced surface disorder on photocatalytic water splitting, ACS Catal. 5 (2015) 1708–1716.

[24] H. Liu, C. Xu, D. Li, H.L. Jiang, Photocatalytic hydrogen production coupled with selective benzylamine oxidation over MOF composites, Angew. Chem. Int. Ed. 57 (2018) 5379–5383.

[25] S. Zhang, W. Huang, X. Fu, X. Zheng, S. Meng, X. Ye, S. Chen, Photocatalytic organic transformations: simultaneous oxidation of aromatic alcohols and reduction of nitroarenes on CdLa$_2$S$_4$ in one reaction system, Appl. Catal. B: Environ. 233 (2018) 1–10.

[26] X. Ning, S. Meng, X. Fu, X. Ye, S. Chen, Efficient utilization of photogenerated electrons and holes for photocatalytic selective organic syntheses in one reaction system using a narrow band gap CdS photocatalyst, Green Chem. 18 (2016) 3628–3639.

[27] L. Jiao, Y. Wang, H.L. Jiang, Q. Xu, Metal-organic frameworks as platforms for catalytic applications, Adv. Mater. 30 (2018) 1–23.

[28] K. Yamaguchi, N. Mizuno, Supported ruthenium catalyst for the heterogeneous oxidation of alcohols with molecular oxygen, Angew. Chem. Int. 41 (2002) 4538–4542.

[29] R. Lin, J. Wan, Y. Xiong, K. Wu, W.C. Cheong, G. Zhou, D. Wang, Q. Peng, C. Chen, Y. Li, Quantitative study of charge carrier dynamics in well-defined WO$_3$ nanowires and nanosheets: insight into the crystal facet effect in photocatalysis, J. Am. Chem. Soc. 140 (2018) 9078–9082.

[30] E. Safaei, S. Mohebbi, Photocatalytic activity of nanohybrid Co-TCPP@TiO$_2$/WO$_3$ in aerobic oxidation of alcohols under visible light, J. Mater. Chem. A 4 (2016) 3933–3946.

[31] S. Yurdakal, G. Palmisano, V. Loddo, O. Alagoz, V. Augugliaro, L. Palmisano, Selective photocatalytic oxidation of 4-substituted aromatic alcohols in water with rutile TiO$_2$ prepared at room temperature, Green Chem. 11 (2009) 510–516.

[32] M.A.S. Andrade, L.H. Mascaro, Photoelectrocatalytic reduction of nitrobenzene on Bi-doped CuGaS$_2$ films, Chemosphere 212 (2018) 79–86.

[33] O.V. Makarova, T. Rajh, M.C. Thurnauer, A. Martin, P.A. Kemme, D. Cropek, Surface modification of TiO$_2$ nanoparticles for photochemical reduction of nitrobenzene, Environ. Sci. Technol. 34 (2000) 4797–4803.

[34] T. Toyao, M. Saito, Y. Horiuchi, K. Mochizuki, M. Iwata, H. Higashimura, M. Matsuoka, Efficient hydrogen production and photocatalytic reduction of nitrobenzene over a visible-light-responsive metal-organic framework photocatalyst, Catal. Sci. Technol. 3 (2013) 2092–2097.

[35] A. Tanaka, Y. Nishino, S. Sakaguchi, T. Yoshikawa, K. Imamura, K. Hashimoto, H. Kominami, Functionalization of a plasmonic Au/TiO$_2$ photocatalyst with an Ag co-catalyst for quantitative reduction of nitrobenzene to aniline in 2-propanol

suspensions under irradiation of visible light, Chem. Commun. 49 (2013) 2551–2553.

[36] Y.F. Li, H.F. Li, T.H. Li, G.L. Li, R. Cao, Facile synthesis of mesoporous titanium dioxide nanocomposites with controllable phase compositions by microwave-assisted esterification, Micropor. Mesopor. Mater. 117 (2009) 444–449.

[37] G. Kresse, J. Furthmuller, Efficient iterative schemes for ab initio total-energy calculations using a plane-wave basis set, Phys. Rev. B 54 (1996) 11169–11186.

[38] G. Kresse, J. Furthmuller, Efficiency of ab-initio total energy calculations for metals and semiconductors using a plane-wave basis set, Comp. Mater. Sci. 6 (1996) 15–50.

[39] G. Kresse, D. Joubert, From ultrasoft pseudopotentials to the projector augmented-wave method, Phys. Rev. B 59 (1999) 1758–1775.

[40] P.E. Blochl, Projector augmented-wave method, Phys. Rev. B 50 (1994) 17953–17979.

[41] J.P. Perdew, K. Burke, M. Ernzerhof, Generalized gradient approximation made simple, Phys. Rev. Lett. 77 (1996) 3865–3868.

[42] H.J. Monkhorst, J.D. Pack, Special points for brillouin-zone integrations, Phys. Rev. B 13 (1976) 5188–5192.

[43] X. Yang, H. Zhao, J. Feng, Y. Chen, S. Gao, R. Cao, Visible-light-driven selective oxidation of alcohols using a dye-sensitized TiO_2-polyoxometalate catalyst, J. Catal. 351 (2017) 59–66.

[44] G. Zhang, G. Kim, W. Choi, Visible light driven photocatalysis mediated via ligand-to-metal charge transfer (LMCT): an alternative approach to solar activation of titania, Energ. Environ. Sci. 7 (2014) 954–966.

[45] H. Park, W. Choi, Effects of TiO_2 surface fluorination on photocatalytic reactions and photoelectrochemical behaviors, J. Phys. Chem. B 108 (2004) 4086–4093.

[46] H.H. Pham, L.W. Wang, Oxygen vacancy and hole conduction in amorphous TiO_2, Phys. Chem. Chem. Phys. 17 (2015) 541–550.

[47] P.S. Kumar, J. Sundaramurthy, S. Sundarrajan, V.J. Babu, G. Singh, S.I. Allakhverdiev, S. Ramakrishna, Hierarchical electrospun nanofibers for energy harvesting, production and environmental remediation, Energy Environ. Sci. 7 (2014) 3192–3222.